ARTICLES

Pten in stromal fibroblasts suppresses mammary epithelial tumours

Anthony J. Trimboli[1,2]*, Carmen Z. Cantemir-Stone[3]*, Fu Li[1,3]*, Julie A. Wallace[3], Anand Merchant[3], Nicholas Creasap[1,2], John C. Thompson[1,2], Enrico Caserta[1,2], Hui Wang[1,2], Jean-Leon Chong[1,2], Shan Naidu[1,2,4], Guo Wei[1,3], Sudarshana M. Sharma[3], Julie A. Stephens[5], Soledad A. Fernandez[5], Metin N. Gurcan[6], Michael B. Weinstein[1,2], Sanford H. Barsky[7]†, Lisa Yee[8], Thomas J. Rosol[4], Paul C. Stromberg[4], Michael L. Robinson[9]†, Francois Pepin[10,11], Michael Hallett[10,11], Morag Park[10,12], Michael C. Ostrowski[3,13] & Gustavo Leone[1,2,13]

The tumour stroma is believed to contribute to some of the most malignant characteristics of epithelial tumours. However, signalling between stromal and tumour cells is complex and remains poorly understood. Here we show that the genetic inactivation of *Pten* in stromal fibroblasts of mouse mammary glands accelerated the initiation, progression and malignant transformation of mammary epithelial tumours. This was associated with the massive remodelling of the extracellular matrix (ECM), innate immune cell infiltration and increased angiogenesis. Loss of *Pten* in stromal fibroblasts led to increased expression, phosphorylation (T72) and recruitment of Ets2 to target promoters known to be involved in these processes. Remarkably, *Ets2* inactivation in *Pten* stroma-deleted tumours ameliorated disruption of the tumour microenvironment and was sufficient to decrease tumour growth and progression. Global gene expression profiling of mammary stromal cells identified a Pten-specific signature that was highly represented in the tumour stroma of patients with breast cancer. These findings identify the Pten–Ets2 axis as a critical stroma-specific signalling pathway that suppresses mammary epithelial tumours.

Coordinated signalling between different cell types of the 'normal stroma' is required during embryonic and adult development[1]. The stroma can be appropriately activated in response to extreme but normal physiological cues, such as wounding, inflammation or pregnancy[2]. The stroma can also be inappropriately activated in cancer[3,4]. In breast tumours, stromal fibroblasts are believed to adapt and continuously co-evolve with tumour epithelial cells to foster transformation and tumour growth[5]. Fibroblasts are a principal constituent of the stroma responsible for the synthesis of growth and survival factors, angiogenic and immunological chemokines, and structural components of the ECM as well as enzymes that control its turnover[6,7]. Despite extensive evidence for a role of the tumour stroma in carcinogenesis, relatively little is known about the signalling pathways involved in the communication between the different cellular compartments of the microenvironment that contribute to the cancer phenotype.

Alterations in the phosphoinositide 3-kinase (PI3K) pathway are associated with the activation of tumour-associated stroma[8,9]. One of the main regulators of PI3K signalling is the phosphatase and tensin homologue (PTEN), a tumour suppressor with lipid and protein phosphatase activity[10,11]. *PTEN* inactivation disrupts multiple cellular processes associated with cell polarity, cell architecture, chromosomal integrity, cell cycle progression, cell growth and stem cell self-renewal[12,13]. Germ-line inactivation of a single allele of *PTEN* in both humans and mice contributes to the genesis of a variety of tumour types of epithelial origin[14]. Although tremendous progress in understanding PTEN function in tumour cells has been made since its discovery over a decade ago, relatively little is known about its potential role in the tumour stroma. Here, we show that *Pten* ablation in mammary stromal fibroblasts of mice results in massive remodelling of the ECM and tumour vasculature, recruitment of innate immune cells and increased malignancy of mammary epithelial tumours. Gene expression profiling of *Pten*-deleted stromal fibroblasts identified the activation of an Ets2-specific transcription program associated with many of these aggressive tumour phenotypes. Remarkably, the concomitant inactivation of *Ets2* in the mammary stroma reversed the increased malignancy caused by *Pten* deficiency. These findings expand Pten's repertoire as a tumour suppressor by identifying the fibroblast as a key site from which it exerts its powerful tumour suppressive influence on the adjacent tumour epithelium.

Stromal *Pten* suppresses mammary epithelial tumours

To evaluate rigorously the role of Pten in the tumour microenvironment of breast cancer, we generated mice containing a mesenchymal-specific *Fsp-cre* transgene[15] and conditional alleles of *Pten* (*Pten*^{loxP}; Supplementary Fig. 1). Cell-type-marker analysis using a β-galactosidase *Rosa26*^{LoxP} reporter allele showed specific *Fsp-cre* expression in stromal fibroblasts surrounding the mammary epithelial ducts, with

[1]Department of Molecular Genetics, College of Biological Sciences, [2]Department of Molecular Virology, Immunology and Medical Genetics, [3]Department of Molecular and Cellular Biochemistry, College of Medicine, [4]Department of Veterinary Biosciences, College of Veterinary Medicine, [5]Center for Biostatistics, Office of Health Sciences, [6]Department of Biomedical Informatics, [7]Department of Pathology and [8]Department of Surgery, School of Medicine, The Ohio State University, Columbus, Ohio 43210, USA. [9]Center for Molecular and Human Genetics, Columbus Children's Research Institute, Columbus, Ohio 43205, USA. [10]Department of Biochemistry, Rosalind and Morris Goodman Cancer Center, [11]McGill Center for Bioinformatics, [12]Department of Oncology, McGill University, Québec H3A 1A1, Canada. [13]Tumor Microenvironment Program, Comprehensive Cancer Center, The Ohio State University, Columbus, Ohio 43210, USA. †Present addresses: Department of Pathology, University of Nevada School of Medicine, Reno, Nevada 89557, and Nevada Cancer Institute, Las Vegas, Nevada 89135, USA (S.H.B.); Department of Zoology, Miami University, Oxford, Ohio 45056, USA (M.L.R.).
*These authors contributed equally to this work.

no expression in cytokeratin-positive epithelial cells, F4/80-positive macrophages and CD31-positive endothelial cells (Fig. 1a and Supplementary Fig. 2a, b). Western blot and PCR assays demonstrated efficient cre-mediated deletion of *Pten*^{loxP} in stromal fibroblasts isolated from *Fsp-cre;Pten*$^{loxP/loxP}$ mammary glands (Fig. 1b and Supplementary Fig. 3a). Examination of mammary sections by immunohistochemistry (IHC) and immunofluorescence showed deletion of *Pten*^{loxP} that was confined to stromal fibroblasts, with no collateral deletion in epithelial ducts or the adjacent myoepithelium (Fig. 1c and Supplementary Fig. 3b, c). Interestingly, this resulted in the expansion of the ECM, but did not lead to the transformation of the mammary epithelium (Fig. 1c, e).

We then examined the role of stromal Pten on mammary tumorigenesis using an established mouse model of breast cancer, *MMTV-ErbB2/neu* (*ErbB2*)[16]. To avoid possible confounding effects caused by *Pten* deletion in mesenchymal cells of other organs, mammary glands from *Fsp-cre;Pten*$^{loxP/loxP}$, *ErbB2;Pten*$^{loxP/loxP}$ and *ErbB2;Fsp-cre;Pten*$^{loxP/loxP}$ donors were transplanted into syngeneic wild-type recipients[17] and tumour development was monitored over the course of several months. By genetically marking the stroma with the *Rosa26*^{LoxP} reporter allele, we demonstrated that both the epithelium and its associated stroma were effectively transplanted into host female mice (Supplementary Fig. 4). Loss of *Pten* in stromal fibroblasts dramatically increased the incidence of *ErbB2*-driven mammary tumours (Fig. 1d–f). By 16 weeks post-transplantation, these lesions progressed to adenoma, carcinoma *in situ* and invasive carcinoma (Fig. 1g), and by 26 weeks most females met the criteria for early removal due to excessive tumour burden (Fig. 1f). Histological examination showed that *ErbB2*-tumour cells in *Pten* stromal-deleted tumours retained their typical oncogene-specific morphology, with small nuclei, fine chromatin and abundant eosinophilic cytoplasm[18]. In contrast to non-deleted tumours[18,19], *Pten* stromal-deleted tumours had a significant amount of stroma surrounding and infiltrating the epithelial masses (Fig. 1g). PCR-based and immunohistochemical assays confirmed that tumours had intact *Pten*^{loxP} alleles in the epithelial compartment (Supplementary Fig. 5a, b and data not shown). Moreover, we used the *Rosa26*^{loxP} reporter allele to mark genetically early epithelial to mesenchymal transition events[15] and found no evidence of epithelial to mesenchymal transition in tumours that either contained or lacked *Pten* in stromal fibroblasts (data not shown). Thus, the analysis of the *ErbB2* breast-cancer tumour model identified a potent tumour suppressor role for Pten in stromal fibroblasts of the mammary gland.

Stromal *Pten* controls ECM and innate immune functions

To investigate the tumour suppressive mechanism of Pten action in stromal fibroblasts, we profiled the transcriptome of mammary stromal fibroblasts isolated from *Pten*$^{loxP/loxP}$ and *Fsp-cre;Pten*$^{loxP/loxP}$ females. Details of sample collection, processing of Affymetrix oligo-arrays and expression data are available in Methods. Briefly, we implemented class comparison analyses of all probe sets on the Affymetrix mouse genome 430 2.0 array to identify genes differentially expressed between the two genetic groups. We also used an unbiased approach similar to gene set enrichment analysis[20] to identify *a priori* defined groups of genes that were significantly differentially expressed. The analysis of over 14,000 mouse genes identified 129 upregulated and 21 downregulated unique genes in response to *Pten* deletion (Supplementary Fig. 6a, b; greater than fourfold at $P < 0.001$; Supplementary Tables 1 and 2). Reverse transcription followed by quantitative PCR (quantitative RT–PCR) assays on a subset of genes confirmed more than 85% of these expression

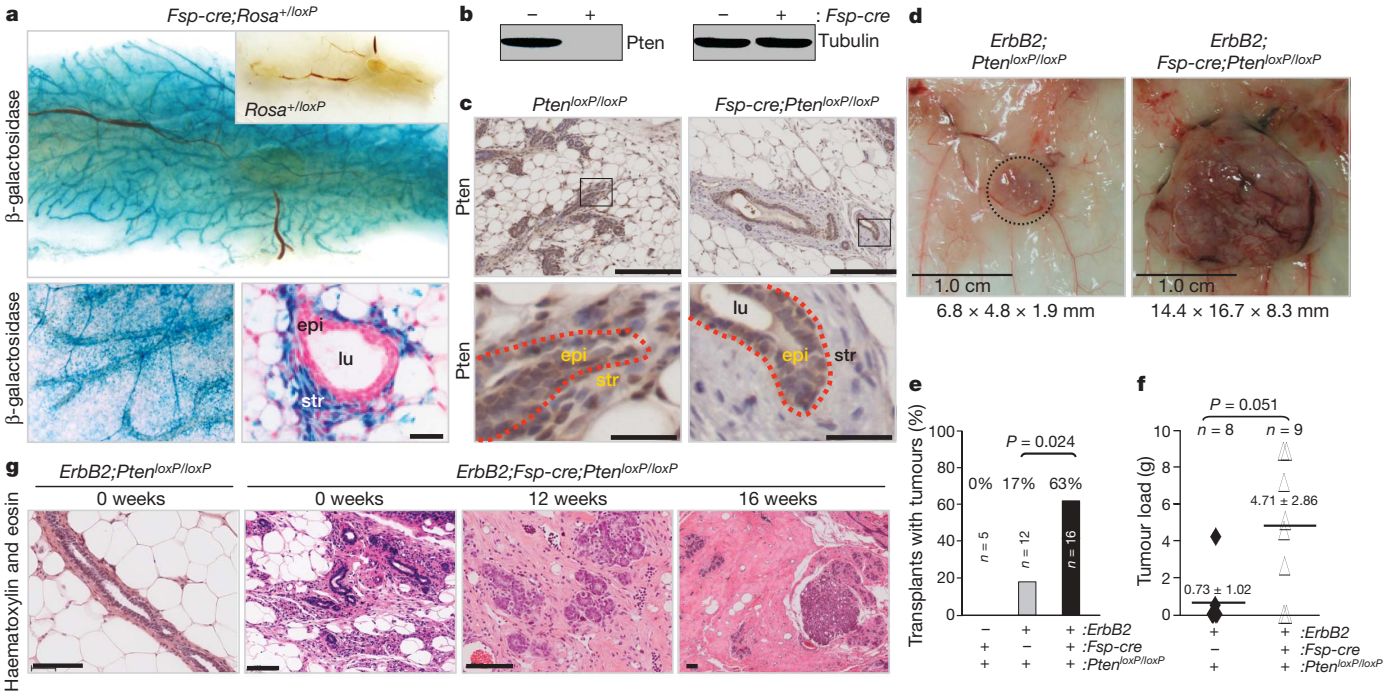

Figure 1 | Stromal fibroblast-specific deletion of *Pten*. **a**, Wholemount, X-gal-stained mammary glands from *Fsp-cre;Rosa*$^{+/loxP}$ and *Rosa*$^{+/loxP}$ (top, inset) mice. Higher magnification of wholemount gland (bottom left) and a histological cross section (bottom right); scale bar, 30 μm. lu, Lumen; epi, epithelium; str, stroma. **b**, Representative western blot analysis of mammary fibroblast lysates derived from 8-week-old *Pten*$^{loxP/loxP}$ mice with (+) or without (−) *Fsp-cre*. **c**, Paraffin sections from 8-week-old female mammary glands stained with a Pten-specific antibody; lower panels represent higher magnifications of boxed areas; scale bars: top panels, 200 μm; bottom panels, 30 μm. lu, Lumen; epi, epithelial compartment; str, stromal compartment; red dotted line indicates the border between the two compartments. **d**, Tumours collected at 26 weeks post-transplantation. **e**, Tumour development by 16 weeks in mammary glands with the indicated genotypes. Tumorigenicity was determined by palpation or histological presentation of adenoma/carcinoma at each implantation site and statistically analysed using Fisher's exact test. *n*, Total number of transplants. **f**, Total tumour burden at 26 weeks post-transplantation in mammary glands with the indicated genotypes. Values represent mean ± s.d. Differences were tested using the non-parametric Wilcoxon rank sum test. **g**, H&E-stained sections of mammary glands harvested at time of transplantation (0 weeks) and indicated times post-transplantation; scale bars, 100 μm.

changes using independent fibroblast samples (Supplementary Fig. 6c and Supplementary Table 3). Fibroblast samples used to probe the oligo-arrays lacked expression of macrophage-, endothelial- and epithelial-specific genes, confirming the purity of these fibroblast preparations (Supplementary Fig. 6d). Functional annotation[21,22] of Pten-responsive targets revealed a remarkable bias towards genes encoding proteins involved in ECM remodelling, wound healing and chronic inflammation[21,22] (Fig. 2a and Supplementary Tables 1 and 2). Given this unexpected convergence of function, we performed a more thorough cellular and molecular analysis of *Pten*-deleted stroma. Staining of consecutive mammary gland sections with haematoxylin and eosin (H&E) and Mason's trichrome stains indicated enhanced deposition of collagen in *Pten*-deleted stroma, which was independent of *ErbB2*-oncogene expression (Fig. 2b, c and Supplementary Fig. 7a). IHC and western blot assays using collagen type-specific antibodies showed that the non-cellular material consisted mostly of type-I collagen and not the basement membrane type-IV collagen (Fig. 2b, c and Supplementary Fig. 7b, c). There was significant infiltration of F4/80-positive macrophages into stromal *Pten*-deleted mammary glands (Fig. 2d, e), and this was independent of *ErbB2* expression (Supplementary Fig. 8a). The abundance of B and T cells did not change in response to stromal deletion of *Pten* (data not shown). From these experiments, we conclude that ablation of *Pten* in stromal fibroblasts recapitulates two key events associated with tumour malignancy: increased ECM deposition and innate immune cell infiltration.

Stromal *Pten* loss activates Ets2

Along with the remarkable remodelling of the tumour microenvironment, loss of *Pten* in stromal fibroblasts resulted in activation of the Ras, JNK and Akt pathways. Western blot analysis using protein lysates derived from *Pten*-deleted stromal fibroblasts demonstrated an increase in the phospho-specific forms of Akt ($Akt^{T308/S473}$) and JNK ($JNK^{T183/Y185}$) (Fig. 2f and Supplementary Fig. 8b). Immunohistochemical assays confirmed the activation of Akt and JNK in stromal fibroblasts, and, interestingly, revealed a profound activation of these two pathways in ductal epithelial cells adjacent to the *Pten*-deleted stroma (Fig. 2g and Supplementary Fig. 8b). This analysis also showed increased levels of phospho-Erk1/2 in *Pten*-deleted stromal fibroblasts; however, this increase could not be detected in primary cultured fibroblasts (Fig. 2f, g), presumably owing to the constitutive Pten-independent activation of Erk1/2 by serum-stimulation[23].

Among the many expression changes observed in *Pten*-deleted stromal fibroblasts we noted that there was a significant increase of *Ets2* messenger RNA (mRNA) levels (2.8-fold, $P < 0.001$). This induction is notable because the Ets2 transcription factor is known to be transcriptionally induced by MAPK[24,25] activation and its function to be post-translationally enhanced by the Akt- and JNK-mediated phosphorylation of its pointed domain at threonine 72 ($Ets2^{T72}$)[23,26]. We confirmed the higher levels of *Ets2* mRNA and protein in *Pten*-deleted fibroblasts (approximately threefold, $P < 0.001$; Supplementary Fig. 9a, b) and, consistent with the activation of Akt and JNK in these mammary glands, there was a marked increase of phospho-$Ets2^{T72}$ in stromal fibroblasts and adjacent epithelial ducts (Fig. 2h, i). Loss of *Pten* in stromal fibroblasts resulted in the induction of several genes involved in ECM remodelling and macrophage recruitment, two of which, *Mmp9* and *Ccl3*, are known to be direct transcriptional targets of Ets2[27,28] (Supplementary Figs 6c and 9c). The increase of *Mmp9* expression appears to be of pathological relevance because *in situ* zymography[29] showed robust Mmp9 activity in tumour samples (Supplementary Fig. 9d). Chromatin immunoprecipitation (ChIP) assays showed an increase in the loading of Ets2 onto the *Mmp9* and *Ccl3* promoters in *Pten*-deleted mammary fibroblasts (Supplementary Fig. 9e), suggesting a direct role for Ets2 in the transcriptional regulation of these two target genes *in vivo*. Together, these data illustrate the extensive molecular reprogramming that takes place in the tumour and its microenvironment in response to ablation of *Pten* in stromal fibroblasts.

Stromal *Ets2* promotes mammary tumorigenesis

To determine whether Ets2 promotes a microenvironment conducive to tumour growth, we analysed the consequences of ablating a conditional allele of *Ets2* ($Ets2^{loxP}$)[30] in mammary stromal fibroblasts of a well-characterized mouse model of breast cancer, *MMTV-PyMT* (*PyMT*)[31]. The *PyMT* oncogene initiates the rapid onset and progression of mammary tumours and thus represents an appropriate model for evaluating any potential delay that loss of *Ets2* might have on tumorigenesis. The efficient *Fsp-cre*-mediated ablation of *Ets2* in stromal fibroblasts was facilitated by using mice carrying conventional and conditional knockout alleles of *Ets2* (DNA binding domain $Ets2^{db/LoxP}$)[32] (Fig. 3a and Supplementary Fig. 10a, b). Ablation of *Ets2* in these cells had no detectable physiological consequence on the development of mammary glands, either during puberty or pregnancy (M.C.O., unpublished observations). The evaluation of $PyMT;Fsp\text{-}cre;Ets2^{db/loxP}$ and control $PyMT;Ets2^{db/loxP}$ mice over a period of three months showed that ablation of *Ets2* in mammary fibroblasts significantly reduced the tumour load (Fig. 3b) and slowed progression to adenoma and early carcinoma (Fig. 3c). Quantitative RT–PCR showed high levels of *Mmp9* expression in tumour-associated fibroblasts containing *Ets2* and low levels in *Ets2*-deleted fibroblasts (Fig. 3e). Because Mmp9 activity is known to mediate the release of matrix-bound VEGF-A to its active isoforms, including $VEGF_{164}$ (ref. 33), we visualized the spatial distribution of $VEGF_{164}$ and Mmp9 activity by immunofluorescence. These assays showed that the accumulation of $VEGF_{164}$, which was particularly acute within collagen-1A-rich stromal locations overlapping Mmp9 activity, was significantly decreased in stromal-deleted *Ets2* tumours (Fig. 3d, f). Given that $VEGF_{164}$ is a specific ligand for VEGF Receptor 2 (VEGFR2; FLK-1; KDR), one of the most potent mediators of VEGF-induced endothelial signalling and angiogenesis[34], we also evaluated VEGFR2 status by immunostaining tumour sections with antibodies specific for CD31 and the phospho-activated form of the murine VEGF receptor ($VEGFR2^{Y1173}$)[35]. This analysis revealed a fourfold decrease in the number of CD31/$VEGFR2^{Y1173}$ double-positive cells in *Ets2*-deleted versus non-deleted tumour samples (Fig. 3f, g). Together, these data show that loss of *Ets2* in stromal fibroblasts results in decreased *Mmp9* activity in the tumour ECM and reduced $VEGFR2^{Y1173}$ activation in the tumour vasculature.

Ets2 is a key component of the stromal *Pten* axis

We then entertained the hypothesis that Ets2 may be contributing to the remodelling of the tumour microenvironment caused by stromal deletion of *Pten*. To test this possibility directly, we compared tumour incidence in $Pten^{loxP/loxP}$, $Fsp\text{-}cre;Pten^{loxP/loxP}$ and $Fsp\text{-}cre;Pten^{loxP/loxP};Ets2^{db/loxP}$ mammary glands that were orthotopically injected with an established *ErbB2*-initiated mammary tumour cell line (NT2.5)[36]. This orthotopic model recapitulated the consequences of deleting *Pten* in the mammary stroma that were observed in the genetically engineered *ErbB2*-mouse model described earlier in this study. Indeed, tumour incidence and tumour load in injected $Fsp\text{-}cre;Pten^{loxP/loxP}$ females was markedly higher than in control $Pten^{loxP/loxP}$ females (Fig. 4a, b). Importantly, mammary glands doubly deleted for stromal *Pten* and *Ets2* had fewer and smaller tumours than glands deleted for *Pten* only. These mammary tumours had decreased numbers of macrophages and recruitment of new vasculature (Fig. 4c–f). Loss of *Pten* and *Ets2*, however, failed to reduce the tumour load and collagen deposition fully to control levels (Fig. 4b and Supplementary Fig. 11a, b), suggesting that additional effectors must contribute towards Pten's tumour suppressor functions. From these data, we conclude that Ets2 is a major component of the Pten tumour-suppressive axis that acts in the stromal fibroblast compartment of mammary glands.

Human breast tumour stroma contains a *Pten* signature

To determine the relevance of these findings to human breast cancer, we compared the mouse stromal fibroblast Pten expression signature

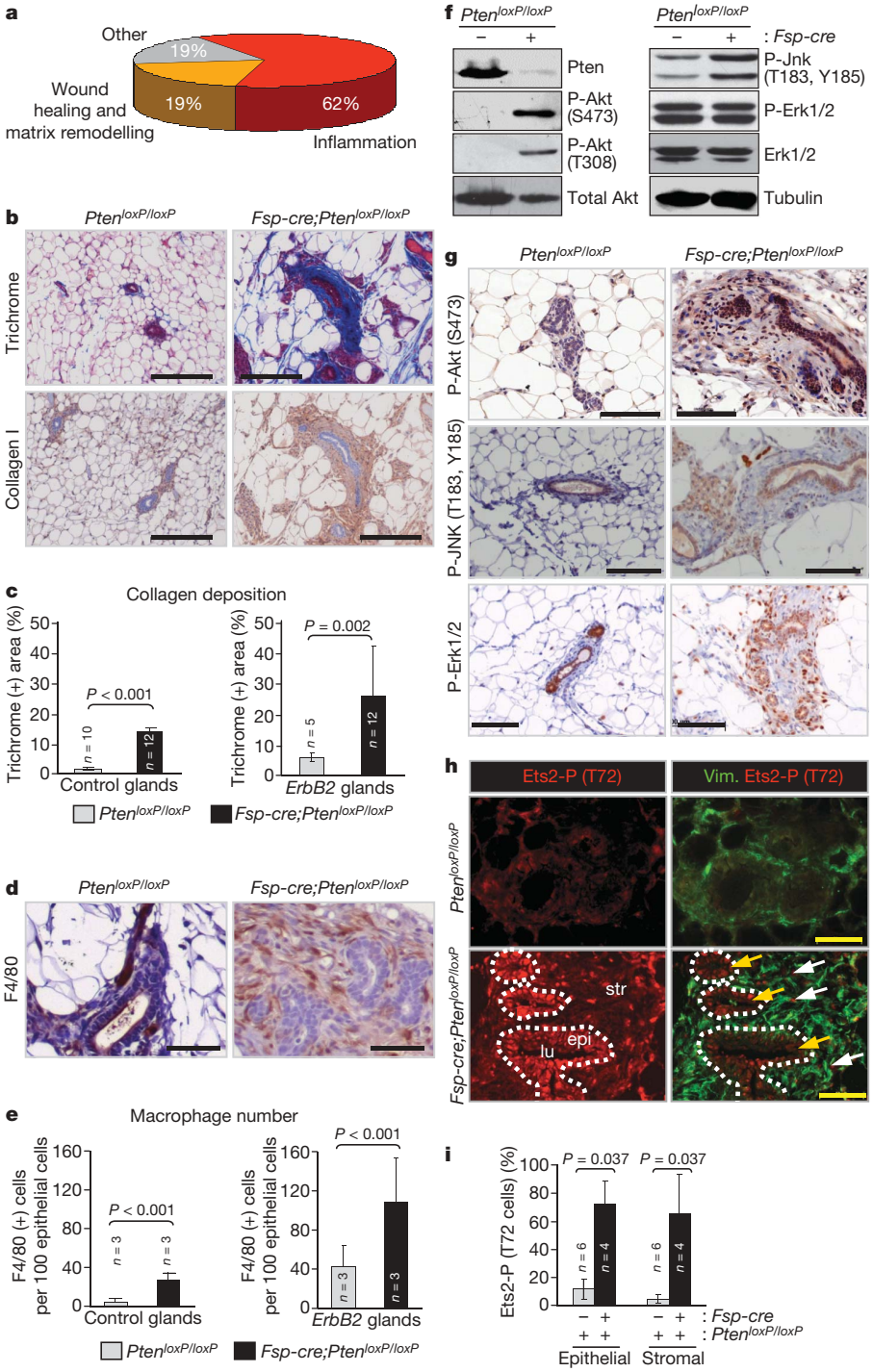

Figure 2 | Characterization of ECM deposition and immune cell infiltration. **a**, Schematic representation of the biological processes affected by differentially expressed genes (more than fourfold) in *Pten*-deleted stromal fibroblasts. **b**, Mammary gland paraffin sections stained with Masson's trichrome and collagen-I-specific antibodies, respectively; scale bars, 200 μm. **c**, Trichrome-stained sections were quantified for collagen deposition; mammary glands in the absence (left) or presence (right) of *ErBb2* were analysed, respectively. Values are means ± s.d.; the Wilcoxon rank sum test was used to compare groups. **d**, Mammary gland paraffin sections stained with the macrophage-specific marker F4/80; scale bars, 50 μm. **e**, Quantification of F4/80-positive stained stromal cells in mammary glands in the absence (left) or presence (right) of *ErBb2*, respectively. Values are means ± s.d.; the Wilcoxon rank sum test was used to compare groups. **f**, Western blot analysis of whole-cell lysates derived from mammary stromal fibroblasts. **g**, Mammary gland paraffin sections stained with phospho-Akt^{S473}-, phospho-JNK$^{T183/Y185}$- and phospho-Erk1/2-specific antibodies; scale bars, 100 μm. All analyses were performed using tissue or cells from 8-week-old females. **h**, Frozen mammary tissue sections stained with vimentin (green) and phospho-Ets2^{T72}-specific (red) antibodies. Note that loss of *Pten* in the mammary stroma increased Ets2 phosphorylation in both the stromal and epithelial compartments. Dotted white line indicates the stromal–epithelial boundary. lu, Lumen; epi, epithelium; str, stroma; scale bars, 50 μm. **i**, Quantification of mammary epithelial and stromal cells that stained positive for nuclear phospho-Ets2^{T72}. Values are means ± s.d.; the Wilcoxon rank sum test was used to compare groups.

to the expression signatures derived from laser-captured tumour stroma (49 samples) and adjacent normal stroma (52 samples) in patients with breast cancer[37]. This analysis identified 137 human orthologues from the 150 differentially expressed mouse genes detected by the Affymetrix oligo-arrays shown in Supplementary Fig. 6a, b. Of these 137 orthologues, 129 genes were represented in

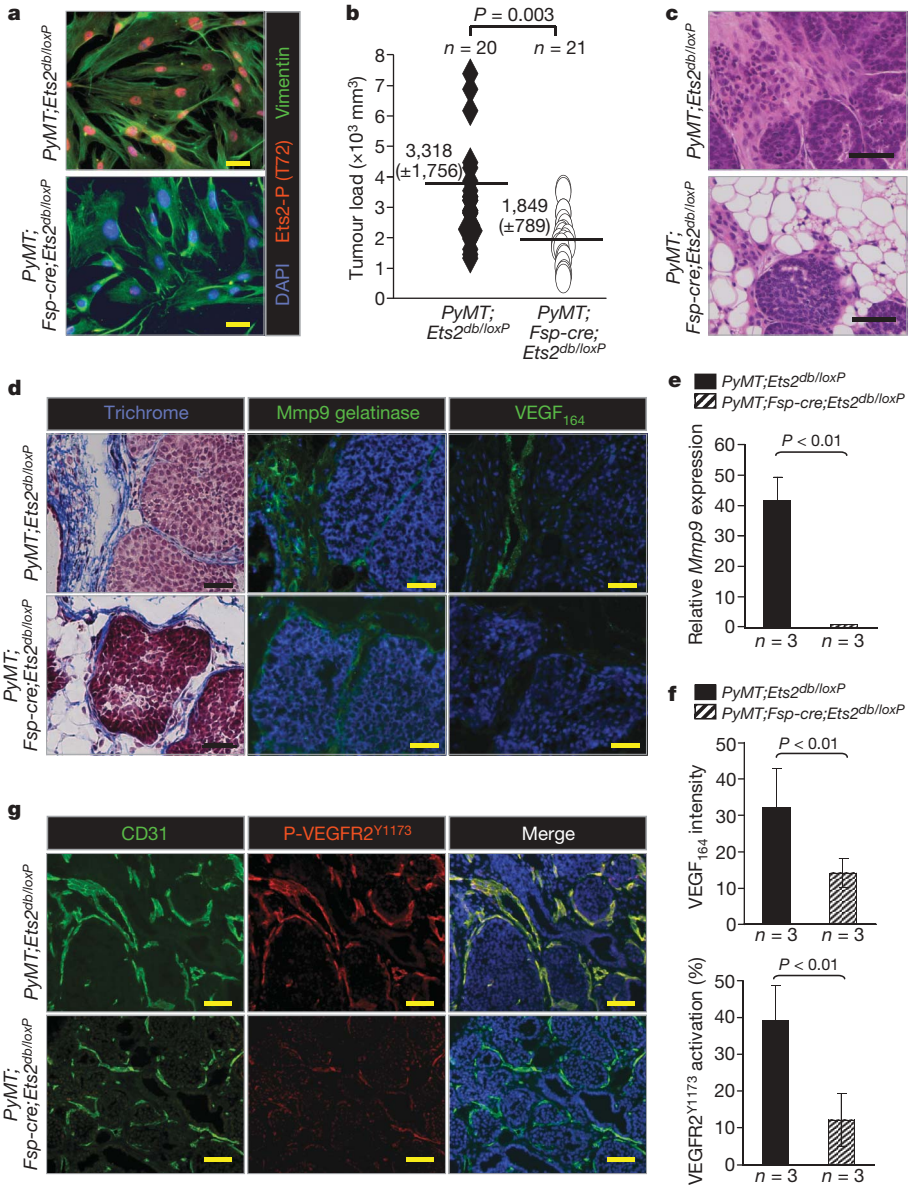

Figure 3 | *Ets2* ablation in stromal fibroblasts restricts mammary tumorigenesis. **a**, Immunofluorescence staining of cultured mammary fibroblasts with vimentin (green), phospho-Ets2^{T72} (red) antibodies and counterstained with 4,6-diamidino-2-phenylindole (DAPI) (blue). **b**, Total mammary tumour volume of *PyMT;Ets2*$^{db/loxP}$ ($n = 20$) and *PyMT;Fsp-cre;Ets2*$^{db/loxP}$ ($n = 21$) mice collected 30 days after tumour initiation. Values represent the mean ± s.d. **c**, H&E staining of tumours harvested from *PyMT;Ets2*$^{db//loxP}$ or *PyMT;Fsp-cre;Ets2*$^{db/loxP}$ mice. **d**, Consecutive sections stained for (left to right): trichrome, Mmp9 gelatinase activity and VEGF$_{164}$, and counterstained with DAPI from *PyMT;Ets2*$^{db/loxP}$ and *PyMT;Fsp-cre;Ets2*$^{db/loxP}$ mammary tumours. **e**, Quantification of *Mmp9* mRNA expression by quantitative RT–PCR. **f**, Quantification of VEGF$_{164}$ immunofluorescence staining in tumour stroma (top) and tumour endothelial cells co-expressing CD31 and phospho-VEGFR2^{Y1173} (bottom). **g**, Tumour vascular endothelial cells visualized by immunofluorescence double staining with CD31 (green) and p-VEGFR2^{Y1173} (red), and counterstained with DAPI (blue) in mammary tumours collected 1 week after tumour initiation in *PyMT;Ets2*$^{db/loxP}$ and *PyMT;Fsp-cre;Ets2*$^{db/loxP}$ mice. All analyses used tissue or cells from 9- to 10-week-old females; scale bars, 50 μm. In **e** and **f**, bars represent means and error bars are s.d. Student's *t*-test was used for all the statistical comparisons between groups.

the expression platform used (Agilent) for the analysis of human patient stroma samples[37]. Only 70 of these 129 genes had highly variable gene expression across all human stromal samples (a variance cutoff of greater than 0.5). The heat map generated for the human stroma data set showed that this 70 gene subset derived from the mouse Pten-signature was sufficient to distinguish normal from tumour stroma in all patients (Fig. 5a; $P = 8 \times 10^{-5}$ as determined by a permutation test). Principal component analysis also discriminated normal from tumour stroma perfectly ($P < 1 \times 10^{-10}$; Supplementary Fig. 12). Interestingly, 12 of the 70 human orthologues identified by the Pten-signature (Fig. 5a: gene names highlighted in red; Supplementary Fig. 13) were previously shown to be differentially expressed in the tumour stroma of patients with breast cancer and to be associated with recurrence[37] (Fig. 5b; $P = 2.5 \times 10^{-8}$, Fisher's exact analysis). These analyses suggest that the fibroblast Pten-expression signature identified by our stromal mouse model represents a significant subset of the total gene signature expressed in the stroma of human breast cancer. We interpret these results to mean that a portion of the transcriptome regulated by Pten in mammary stromal fibroblasts is dysregulated in the tumour stroma of patients with breast cancer.

We also evaluated the relevance of the Pten–Ets2 relationship in human cancer by immunohistochemical staining of breast-cancer tissue microarrays (TMAs) with antibodies specific for Pten, P-Ets2^{T72} and P-Akt^{S473} (Fig. 5c). From the analysis of 99 patient samples with invasive carcinoma, PTEN expression was scored as

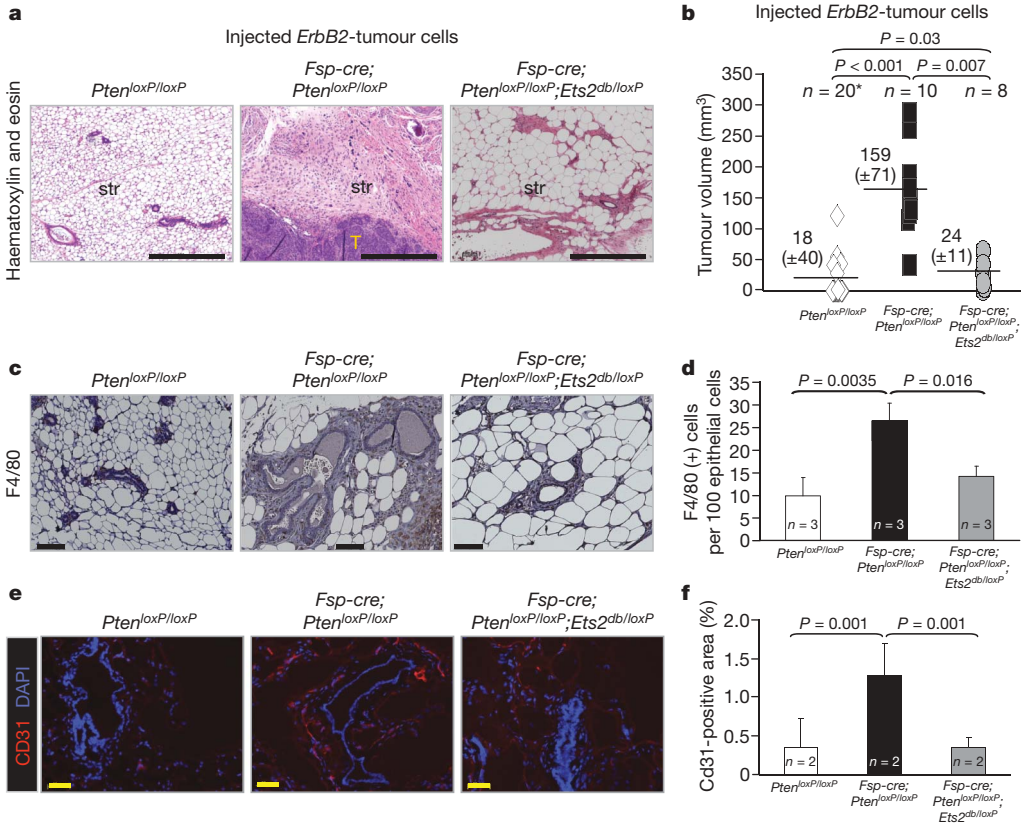

Figure 4 | Loss of *Ets2* in stromal fibroblasts diminishes tumour growth in stromal *Pten*-deleted mammary glands. **a**, H&E sections of mammary glands after orthotopic injection of the *ErbB2*-expressing tumour cell line NT2.5. T, tumour; str, stroma; scale bars, 500 μm. **b**, Volumes of tumours collected 21 days after injection. $Pten^{loxP/loxP};Ets2^{db/loxP}$ ($n = 10$) and $Pten^{loxP/loxP}$ ($n = 10$) control groups were combined (*, $n = 20$) after it was determined that there was no statistical difference in tumour incidence or load between these two control groups. Values are means ± s.d. **c**, Sections from mammary glands with the indicated genotypes stained with the macrophage-specific marker F4/80. Scale bars, 100 μm. **d**, Quantification of stromal cells positive for F4/80 in mammary glands. **e**, Frozen mammary gland sections stained with the endothelial-specific antibody, CD31. Scale bars, 50 μm. **f**, Quantification of CD31-positive staining. In **d** and **f**, bars represent means and error bars are s.d. For all the statistical analyses, an analysis of variance model with Bonferroni adjustment was used. Pairwise comparisons shown have a significant difference between marked genetic groups.

absent or low in approximately 50% of samples. Importantly, PTEN staining in the TMAs was negatively correlated with P-AKT^{S473} and nuclear P-ETS2^{T72}, whereas P-AKT^{S473} and nuclear P-ETS2^{T72} showed a positive association (Fig. 5d). These results suggest that activation of P-ETS2^{T72} in human breast-cancer stroma is a pathological event that is favoured by a reduction in PTEN expression.

Discussion

Histopathology and molecular studies suggest that malignant tumours consist of a complex cellular system that is dependent on reciprocal signalling between tumour cells and the adjacent stroma. However, the signalling pathways that mediate the communication between the various cell types in the tumour remain virtually unknown. We recently developed a mesenchymal-specific *cre* mouse[15] and used it here to examine the consequences of inactivating *Pten* in mammary stromal fibroblasts. Using this system we show, for the first time to our knowledge, that *Pten* in stromal fibroblasts has a critical role in the suppression of epithelial mammary tumours that is, in part, mediated through an Ets2-regulated transcriptional program.

The tumour suppressor functions of PTEN have been extensively studied in the tumour cell[38–40]. We show here that genetic ablation of *Pten* in mammary stromal fibroblasts of mice alters the expression profile of these cells to increase ECM, chemokine and cytokine production in the tumour microenvironment. As a result, *Pten* stromal-deleted tumours exhibit high levels of collagen, macrophage recruitment and vascular networks, which together favour the initiation and progression of mammary epithelial tumours. Remarkably, side-by-side evaluation of histopathology by independent pathologists could not distinguish tumours between *Pten* stromal-deleted mice and human patients with breast cancer, highlighting the importance of modelling stromal cell compartments of the tumour microenvironment. The mechanism by which Pten in the stroma likely exerts its tumour suppressor role is through the control of multiple signalling pathways, including components of the Ras, Akt and JNK networks, which together culminate in the regulation of Ets2 transcriptional activity. The fact that loss of *Ets2* in mammary stromal fibroblasts diminished the oncogenic consequences of deleting *Pten* in these cells underscores the importance of the stromal Pten–Ets2 axis in stromal fibroblasts during tumour suppression. These observations are consistent with previous work from Oshima and colleagues that showed a critical cell non-autonomous role for *Ets2* in the growth of mammary tumours in mice[41] and with the identification of Ets2 activation as a key event associated with breast cancer in human patients having poor prognosis[42–44]. The relevance of this mouse Pten–Ets2 tumour suppressor axis to breast cancer is underlined by the high correspondence between the mouse and human stromal expression signatures. The observation that the dire consequences of targeting this Ets2-driven stromal program are tumour-specific, sparing normal mammary development, emphasizes the potential use of stromal-specific strategies for therapeutic intervention in human breast cancer.

In summary, this work identifies Pten–Ets2 as a key regulatory axis in stromal fibroblasts that suppresses mammary epithelial tumours by profoundly attenuating some of the most malignant characteristics of the tumour microenvironment. This novel function of Pten may be relevant in the suppression of epithelial tumours of other organs, but may also extend beyond cancer, to conditions where the microenvironment may impact disease manifestation, such as in autoimmune

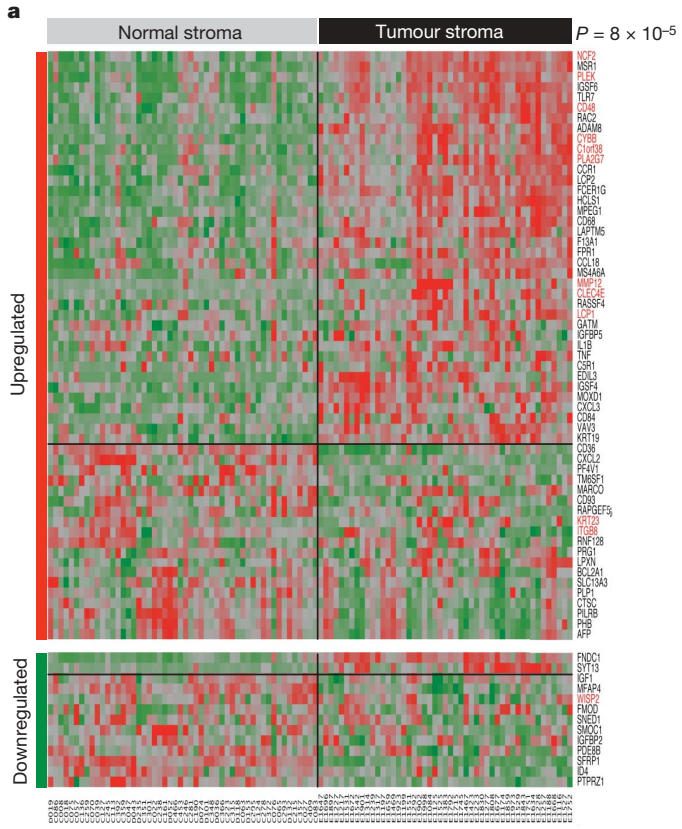

d

Correlation between:	Pearson	*P*
PTEN and ETS2-P (T72)	−0.577	< 0.001
PTEN and AKT-P (S473)	−0.552	< 0.001
ETS2-P (T72) and AKT-P (S473)	0.947	< 0.001

Figure 5 | Pten-signature is represented in breast cancer stroma. a, Heat map displaying the expression of the human orthologues of the 70-gene subset in normal- and tumour-stroma from human patients with breast cancer. The 70-gene subset derived from the mouse Pten-signature includes 57 genes upregulated (red bar on *y*-axis) and 13 genes downregulated (green bar on *y*-axis). Red and green regions inside the heat map indicate relative gene expression levels (red, increased; green, decreased). The *P* value indicates the ability of the mouse 70-gene signature to partition normal and tumour stroma in patients with breast cancer (see Statistical Methods). The coded patient identities are listed at the bottom. **b**, Venn diagram depicting the overlap between the mouse *Pten*-deleted fibroblast and human stroma microarray data sets. The 12 genes highlighted in red (**a**, right margin) are common between the mouse Pten 70-gene signature and the human 163-gene signature that has been shown to associate with recurrence[38]. This overlap is highly significant ($P = 2.5 \times 10^{-8}$; Fisher's exact test). **c**, Representative PTEN, P-ETS2^{T72} and P-AKT^{S473} IHC staining in human breast carcinoma samples from the tissue microarray. Scale bar, 50 μm. **d**, Pearson correlations between PTEN , P-ETS2^{T72} and P-AKT^{S473} expression based on Allred scores of a tissue microarray (**c**) containing 99 patients with advanced breast carcinoma.

syndromes[45], lung fibrosis[46] and neurodegeneration[47]. Interestingly, the stromal Pten expression signature identified here includes genes that have been causally linked to ECM deposition and inflammation in rheumatoid arthritis, lung fibrosis and neurodegeneration (Supplementary Tables 1 and 2). These data offer a molecular basis for how altered Pten signalling in the tumour stroma may elicit broad responses in a variety of cells in the tumour microenvironment that contribute to disease manifestation.

METHODS SUMMARY

Transgenic mice. Generation of *Fsp-cre* mice has been described[15]. *Pten*^{loxP} mice were created following the strategy described in Supplementary Fig. 1. *Ets2*^{loxP} mice were generated by standard techniques[30]. Animals were maintained and killed following institutional guidelines. Tenth-generation congenic (N10) FVB/N animals were used for transplantation and orthotopic injection studies.

Tissue processing, histology. Tissues were either embedded in OCT or fixed (4% paraformaldehyde or formalin) and embedded in paraffin. Frozen sections were used for X-gal staining as previously described[15]. IHC on tissue microarray sections from 99 patients with breast carcinoma was scored using Allred score's system[48].

Isolation of primary mammary fibroblasts. Primary mammary fibroblasts were purified following the protocol published previously with minor modifications[49]. Mammary glands were dissected from 8-week-old female mice, minced and digested with collagenase (0.15% Collagenase I, 160 U ml^{-1} hyaluonidase, 1 μg ml^{-1} hydrocortisone and 10 μg ml^{-1} insulin with penicillin and streptomycin) in a 5% CO_2 incubator overnight at 37 °C. Collagenase was neutralized with 10% FBS–DMEM medium. Digested tissue was resuspended in medium and subjected to gravity for 12–15 min. Pellets were washed three times to collect epithelial organoids, and supernatants were subjected four more times to gravity sedimentation and then cultured.

RNA and microarray analysis. RNA was harvested with Trizol according to the manufacturer's instructions (Invitrogen). RNA quality and concentration were assessed with Bioanalyser and Nanodrop RNA 6000 nano-assays. RNA samples were hybridized to Affymetrix GeneChip Mouse genome 430 2.0 platform at the Microarray Shared Resource Facility, Ohio State University Comprehensive Cancer Center. The microarray data were deposited with Gene Expression Omnibus (GEO) and can be viewed at http://www.ncbi.nlm.nih.gov/geo/query/acc.cgi?token=zhmbrcoqaacyite&acc=GSE16073.

Full Methods and any associated references are available in the online version of the paper at www.nature.com/nature.

Received 29 May; accepted 7 September 2009.

1. Wiseman, B. S. & Werb, Z. Stromal effects on mammary gland development and breast cancer. *Science* **296,** 1046–1049 (2002).
2. Nelson, C. M. & Bissell, M. J. Of extracellular matrix, scaffolds, and signaling: tissue architecture regulates development, homeostasis, and cancer. *Annu. Rev. Cell Dev. Biol.* **22,** 287–309 (2006).
3. Mueller, M. M. & Fusenig, N. E. Friends or foes – bipolar effects of the tumour stroma in cancer. *Nature Rev. Cancer* **4,** 839–849 (2004).
4. Schedin, P. Pregnancy-associated breast cancer and metastasis. *Nature Rev. Cancer* **6,** 281–291 (2006).
5. Littlepage, L. E., Egeblad, M. & Werb, Z. Coevolution of cancer and stromal cellular responses. *Cancer Cell* **7,** 499–500 (2005).
6. Bhowmick, N. A., Neilson, E. G. & Moses, H. L. Stromal fibroblasts in cancer initiation and progression. *Nature* **432,** 332–337 (2004).
7. Kalluri, R. & Zeisberg, M. Fibroblasts in cancer. *Nature Rev. Cancer* **6,** 392–401 (2006).
8. Cully, M., You, H., Levine, A. J. & Mak, T. W. Beyond PTEN mutations: the PI3K pathway as an integrator of multiple inputs during tumorigenesis. *Nature Rev. Cancer* **6,** 184–192 (2006).
9. Bergamaschi, A. *et al.* Extracellular matrix signature identifies breast cancer subgroups with different clinical outcome. *J. Pathol.* **214,** 357–367 (2008).
10. Myers, M. P. *et al.* The lipid phosphatase activity of PTEN is critical for its tumor supressor function. *Proc. Natl Acad. Sci. USA* **95,** 13513–13518 (1998).
11. Stambolic, V. *et al.* Negative regulation of PKB/Akt-dependent cell survival by the tumor suppressor PTEN. *Cell* **95,** 29–39 (1998).
12. Salmena, L., Carracedo, A. & Pandolfi, P. P. Tenets of PTEN tumor suppression. *Cell* **133,** 403–414 (2008).
13. Knobbe, C. B., Lapin, V., Suzuki, A. & Mak, T. W. The roles of PTEN in development, physiology and tumorigenesis in mouse models: a tissue-by-tissue survey. *Oncogene* **27,** 5398–5415 (2008).
14. Di Cristofano, A., Pesce, B., Cordon-Cardo, C. & Pandolfi, P. P. *Pten* is essential for embryonic development and tumour suppression. *Nature Genet.* **19,** 348–355 (1998).
15. Trimboli, A. J. *et al.* Direct evidence for epithelial–mesenchymal transitions in breast cancer. *Cancer Res.* **68,** 937–945 (2008).
16. Guy, C. T. *et al.* Expression of the neu protooncogene in the mammary epithelium of transgenic mice induces metastatic disease. *Proc. Natl Acad. Sci. USA* **89,** 10578–10582 (1992).
17. Cases, S. *et al.* Development of the mammary gland requires DGAT1 expression in stromal and epithelial tissues. *Development* **131,** 3047–3055 (2004).

18. Andrechek, E. R. *et al.* Amplification of the neu/erbB-2 oncogene in a mouse model of mammary tumorigenesis. *Proc. Natl Acad. Sci. USA* **97,** 3444–3449 (2000).
19. Desai, K. V. *et al.* Initiating oncogenic event determines gene-expression patterns of human breast cancer models. *Proc. Natl Acad. Sci. USA* **99,** 6967–6972 (2002).
20. Mootha, V. K. *et al.* PGC-1α-responsive genes involved in oxidative phosphorylation are coordinately downregulated in human diabetes. *Nature Genet.* **34,** 267–273 (2003).
21. Dennis, G., Jr *et al.* DAVID: Database for Annotation, Visualization, and Integrated Discovery. *Genome Biol.* **4,** 3 (2003).
22. Huang, D. W., Sherman, B. T. & Lempicki, R. A. Systematic and integrative analysis of large gene lists using DAVID bioinformatics resources. *Nature Protocols* **4,** 44–57 (2009).
23. Weng, L. P., Brown, J. L., Baker, K. M., Ostrowski, M. C. & Eng, C. PTEN blocks insulin-mediated ETS-2 phosphorylation through MAP kinase, independently of the phosphoinositide 3-kinase pathway. *Hum. Mol. Genet.* **11,** 1687–1696 (2002).
24. Fowles, L. F. *et al.* Persistent activation of mitogen-activated protein kinases p42 and p44 and ets-2 phosphorylation in response to colony-stimulating factor 1/c-fms signaling. *Mol. Cell. Biol.* **18,** 5148–5156 (1998).
25. McCarthy, S. A. *et al.* Rapid phosphorylation of Ets-2 accompanies mitogen-activated protein kinase activation and the induction of heparin-binding epidermal growth factor gene expression by oncogenic Raf-1. *Mol. Cell. Biol.* **17,** 2401–2412 (1997).
26. Smith, J. L. *et al.* ets-2 is a target for an akt (Protein kinase B)/jun N-terminal kinase signaling pathway in macrophages of motheaten-viable mutant mice. *Mol. Cell. Biol.* **20,** 8026–8034 (2000).
27. Watabe, T. *et al.* The Ets-1 and Ets-2 transcription factors activate the promoters for invasion-associated urokinase and collagenase genes in response to epidermal growth factor. *Int. J. Cancer* **77,** 128–137 (1998).
28. Wei, G. *et al.* Activated Ets2 is required for persistent inflammatory responses in the motheaten viable model. *J. Immunol.* **173,** 1374–1379 (2004).
29. Ludwig, T. Local proteolytic activity in tumor cell invasion and metastasis. *Bioessays* **27,** 1181–1191 (2005).
30. Wei, G. *et al.* Ets1 and Ets2 are required for endothelial cell survival during embryonic angiogenesis. *Blood* **114,** 1123–1130 (2009).
31. Lin, E. Y. *et al.* Progression to malignancy in the polyoma middle T oncoprotein mouse breast cancer model provides a reliable model for human diseases. *Am. J. Pathol.* **163,** 2113–2126 (2003).
32. Yamamoto, H. *et al.* Defective trophoblast function in mice with a targeted mutation of Ets2. *Genes Dev.* **12,** 1315–1326 (1998).
33. Lee, S., Jilani, S. M., Nikolova, G. V., Carpizo, D. & Iruela-Arispe, M. L. Processing of VEGF-A by matrix metalloproteinases regulates bioavailability and vascular patterning in tumors. *J. Cell Biol.* **169,** 681–691 (2005).
34. Millauer, B. *et al.* High affinity VEGF binding and developmental expression suggest Flk-1 as a major regulator of vasculogenesis and angiogenesis. *Cell* **72,** 835–846 (1993).
35. Sakurai, Y., Ohgimoto, K., Kataoka, Y., Yoshida, N. & Shibuya, M. Essential role of Flk-1 (VEGF receptor 2) tyrosine residue 1173 in vasculogenesis in mice. *Proc. Natl Acad. Sci. USA* **102,** 1076–1081 (2005).
36. Dakappagari, N. K. *et al.* Conformational HER-2/neu B-cell epitope peptide vaccine designed to incorporate two native disulfide bonds enhances tumor cell binding and antitumor activities. *J. Biol. Chem.* **280,** 54–63 (2005).
37. Finak, G. *et al.* Stromal gene expression predicts clinical outcome in breast cancer. *Nature Med.* **14,** 518–527 (2008).
38. Berns, K. *et al.* A functional genetic approach identifies the PI3K pathway as a major determinant of trastuzumab resistance in breast cancer. *Cancer Cell* **12,** 395–402 (2007).
39. Saal, L. H. *et al.* Recurrent gross mutations of the PTEN tumor suppressor gene in breast cancers with deficient DSB repair. *Nature Genet.* **40,** 102–107 (2008).
40. Saal, L. H. *et al.* Poor prognosis in carcinoma is associated with a gene expression signature of aberrant PTEN tumor suppressor pathway activity. *Proc. Natl Acad. Sci. USA* **104,** 7564–7569 (2007).
41. Tynan, J. A., Wen, F., Muller, W. J. & Oshima, R. G. Ets2-dependent microenvironmental support of mouse mammary tumors. *Oncogene* **24,** 6870–6876 (2005).
42. Buggy, Y. *et al.* Ets2 transcription factor in normal and neoplastic human breast tissue. *Eur. J. Cancer* **42,** 485–491 (2006).
43. Park, E. S. *et al.* Heterologous tissue culture expression signature predicts human breast cancer prognosis. *PLoS One* **2,** e145 (2007).
44. Svensson, S. *et al.* ERK phosphorylation is linked to VEGFR2 expression and Ets-2 phosphorylation in breast cancer and is associated with tamoxifen treatment resistance and small tumours with good prognosis. *Oncogene* **24,** 4370–4379 (2005).
45. Pap, T. *et al.* Activation of synovial fibroblasts in rheumatoid arthritis: lack of Expression of the tumour suppressor PTEN at sites of invasive growth and destruction. *Arthritis Res.* **2,** 59–64 (2000).
46. White, E. S. *et al.* Negative regulation of myofibroblast differentiation by PTEN (phosphatase and tensin homolog deleted on chromosome 10). *Am. J. Respir. Crit. Care Med.* **173,** 112–121 (2006).
47. Gibson, G. E. & Huang, H. M. Oxidative processes in the brain and non-neuronal tissues as biomarkers of Alzheimer's disease. *Front. Biosci.* **7,** d1007–d1015 (2002).
48. Allred, D. C., Harvey, J. M., Berardo, M. & Clark, G. M. Prognostic and predictive factors in breast cancer by immunohistochemical analysis. *Mod. Pathol.* **11,** 155–168 (1998).
49. Soule, H. D. & McGrath, C. M. A simplified method for passage and long-term growth of human mammary epithelial cells. *In Vitro Cell. Dev. Biol.* **22,** 6–12 (1986).

Supplementary Information is linked to the online version of the paper at www.nature.com/nature.

Acknowledgements We thank M. Rawahneh and J. Moffitt for histotechnical assistance, K. Kornacker, S. Cory and I. Vasudeva Murthy for bioinformatics assistance, P. Gulati for statistics assistance, the Ohio State University Human Tissue Resource Network and the Ohio State University Comprehensive Cancer Center Microarray, Nucleic Acids, Trangenics and Flow Cytometry Shared Facilities for technical assistance. *MMTV-ErbB2* mice were provided by W. Muller. This work was funded by the National Institutes of Health to G.L. (R01CA85619, R01HD47470, P01CA097189) and to M.C.O. (R01CA053271, P01CA097189), by the Komen Breast Cancer Foundation and Evelyn Simmers Charitable Trust to M.C.O., by the Terry Fox New Frontiers Group Grant to M.P., and by the Natural Science and Engineering Research Council of Canada Discovery Grants Program grant to M.H. F.L. and F.P. were funded by Department of Defense Pre-doctoral Fellowships and J.-L.C. was funded by a Department of Defense Postdoctoral Fellowship. G.L. is the recipient of the Pew Charitable Trusts Scholar Award and the Leukemia and Lymphoma Society Scholar Award. M.P. holds the Diane and Sal Guerrera Chair in Cancer Genetics at McGill University.

Author Contributions G.L. and M.C.O. designed and supervised this study, analysed data, and helped write and edit the manuscript. A.J.T., C.Z.C., F.L. and J.A.W. designed and performed experiments, collected and analysed data, and co-wrote the paper. N.C., J.C.T., H.W., J-L.C., S.M.S. and M.N.G. technically assisted with experiments, and collected and analysed data. G.W., A.J.T., M.L.R and M.W performed experiments in initial stages of the project, particularly in designing and characterizing the mouse models. S.N., P.S. and T.J.R. contributed to the histopathological analysis of the mouse mammary tumour models and writing the manuscript. S.H.B. and L.Y. contributed to the histopathological analysis of human samples and writing the manuscript. S.A.F. and J.A.S. contributed to the statistical analyses of data and writing the manuscript. A.M., F.P., J.A.W., E.C., M.H. and M.P. contributed to the analysis and comparison of mouse and human microarray data and writing the mansucript.

Author Information Reprints and permissions information is available at www.nature.com/reprints. Correspondence and requests for materials should be addressed to M.C.O. (michael.ostrowski@osumc.edu) or G.L. (gustavo.leone@osumc.edu).

METHODS

Transgenic mice. Animals were housed according to federal and University Laboratory Animal Resources at Ohio State University regulations.

Fsp-cre: the generation of the *Fsp-cre* mouse line has been previously described[15].

Ets2^{loxP}: the *Ets2* conditional transgenic mouse line was generated such that the *Ets2* pointed domain is 'floxed'[28]. The pointed domain is encoded by exons 3–5 and important for the protein–protein interaction and signal transduction.

Ets2^{db}: the *Ets2*^{db} mouse was a gift from R. G. Oshima[32].

Pten^{loxP}: the *Pten*^{loxP} mice were generated in our laboratory. *LoxP* sites were introduced into two *Hpa*I sites within introns 3 and 5 of the *Pten* gene, respectively, to flank exons 4 and 5. Exon 5 encodes the lipid phosphatase domain. Tissue-specific expression of *cre* will excise exons 4 and 5, generating a loss-of-function *Pten*$^{\Delta}$ allele (Supplementary Fig. 1).

Rosa-LacZ: the generation of the conditional *Rosa-LacZ* mouse line has been previously described[50]. A list of PCR primers can be found in Supplementary Table 3.

Mammary tissue transplantation. Transplant procedure was based on a previously published method[17]. The day before surgery, recipient mice were anaesthetized with isofluorane (Abbott Laboratories) and a square area along the scapular region was shaved (roughly 25 mm × 25 mm). At the time of surgery, inguinal and groin mammary tissue (approximately 5 mm × 5 mm in size) was removed from 8- to 9-week-old donor females and placed subcutaneously into the scapular region of wild-type hosts (littermates or FVB/N purchased from Taconic) through two 5- to 10-mm incisions on the left and right side under aseptic conditions. Only tissue from the abdominal (#4 and #9) and groin (#5 and #10) mammary glands was used for transplant after the lymph nodes were removed. The small incisions were closed using a 9-mm wound clip. Animals were monitored twice a week until tumour onset. Mice were killed either at specific time points, when the tumour was about 2 cm in size, or it presented a health problem to the animal such as exterior ulceration at the site of the tumour.

Orthotopic mammary gland injection. The neu-expressing mouse mammary carcinoma cell line NT2.5 was provided by P. T. Kaumaya and was maintained as described[36]. Eight-week-old female mice of each genotype were anaesthetized and injected with 5×10^5 NT2.5 cells at both inguinal mammary glands. Tumour initiation was monitored by palpating twice a week. All the mice were killed three weeks after injection. Tumour volume was calculated by the formula $V = ½ \times \text{length} \times (\text{width})^2$.

Tissue processing and X-gal staining. Large individual tumours (typically ~1–2 cm) or the remainder of transplanted tissues were removed, divided and either fixed in 4% paraformaldehyde for 24–48 h or embedded directly in OCT (Sakura). Fixed tissue samples were embedded in paraffin and cut into 5-μm sections for H&E, IHC or immunofluorescence staining. For each sample collected, two sets of sections were obtained at 25-μm intervals for analysis. Corresponding OCT-embedded tissue was sectioned (7 μm) in a similar manner for X-gal or immunofluorescence staining. For X-gal staining, frozen tissue sections were dried 15 min at room temperature before fixing in a glutaraldehyde solution (0.2% glutaraldehyde, 1.25 mM EGTA, pH 7.3 and 2 mM magnesium chloride in 1 × PBS) for 30 min. The sections were washed with LacZ wash buffer (2 mM magnesium chloride, 0.01% sodium deoxycholate, 0.02% IGEPAL CA-630 (Sigma) in PBS) for 5 min three times and then stained in LacZ staining solution (4 mM potassium ferricyanide, 4 mM potassium ferrocyanide, 1 mg ml^{-1} X-gal in LacZ wash buffer) at 37 °C overnight (~18 h) and protected from light. Stained sections were washed in PBS for 5 min three times and then rinsed with water for 2 min before counter-staining with nuclear fast red. Collagen deposition was visualized using standard Masson's trichrome staining. Whole mammary gland sections were stained and imaged using an Aperio Scanscope CS whole-slide scanner. Areas of skin and muscle, which also stain positive, were manually encircled and excluded from the analysis.

IHC and immunofluorescence. IHC and immunofluorescence were performed using paraffin sections with the following antibodies: Pten (1:100, Cell Signaling, overnight), collagen I (1:100, Abcam, 30 min), F4/80 (1:50, Caltag, overnight), phospho-Akt^{S473} (1:50, Cell Signaling, overnight), phospho-JNK$^{T183/Y185}$ (1:50, Cell Signaling, overnight), phospho-Erk1/2 (1:100, Cell Signaling, overnight), phospho-Ets2^{T72} (1:25, M.C.O. laboratory, overnight), Cytokeratin 8/18 (1:300; Research Diagnostics, 30 min), E-cadherin (1:700, BD-Pharmingen, 30 min), mouse α-SMA (1:200, Sigma, 30 min) and collagen IV (1:100, Chemicon, 30 min). In general, paraffin sections were deparaffinized and the antigen retrieval accomplished by incubation in antigen retrieval solution (DAKO) at >95 °C (30 min). For IHC, staining was developed using the biotin/avidin/horseradish peroxidase system from Vector Laboratories according to the manufacturer's instructions. All IHC slides were counterstained with haematoxylin and images obtained using an Eclipse 50i microscope (Nikon) and an Axiocam HRc camera (Zeiss). For IHC quantification, cells were counted manually from ten random fields and reported as a percentage of positive cells from the total cell population.

Frozen sections of mammary glands for immunofluorescence were fixed at 4 °C in either 4% paraformaldehyde in PBS or acetone. Samples were treated with phospho-Ets2^{T72} (1:125; M.C.O. laboratory, overnight), vimentin (1:50; Santa Cruz Biotech, overnight), Pten (1:100, Cell Signaling, overnight), $VEGF_{164}$ (1:100, R&D Systems, overnight), phospho-VEGFR2^{Y1173} (1:100, Cell Signaling, overnight) and CD31 (1:50, BD Biosciences, 30 min) primary antibodies. Fluorescent staining was developed using secondary antibodies conjugated to AlexaFluor dyes following standard protocol (Invitrogen; Molecular Probes). For Pten immunofluorescence on paraffin sections, the signal was amplified using a biotinylated secondary antibody and Texas red conjugated to streptavidin. All immunofluorescence sections were counterstained with DAPI and images obtained using an Axioscope 40 microscope (Zeiss) equipped with an Axiocam HRc camera (Zeiss). Image analysis for quantifying CD31 and phospho-VEGFR2^{Y1173} areas was performed using standard image processing techniques implemented in Matlab. $VEGF_{164}$ images were quantified with ImageJ software.

Gelatinase *in situ* zymography. This was performed as described, with minor modification[51]. Briefly, frozen sections (10 μm) were quickly fixed with cold acetone, rehydrated with PBS and then incubated with 40 μg ml^{-1} DQ-gelatin fluorescein conjugate (Molecular Probes) in reaction buffer (50 mM Tris-HCl, 150 mM NaCl, 5 mM $CaCl_2$ and 0.2 mM NaN_3, pH 7.6) for 10 h. The reaction was quenched with 10 mM EDTA-PBS wash. Nuclei were counterstained with DAPI. A consecutive slide was stained with H&E to localize the MMP9 activity. Fluorescent images were acquired with Axioscope40 microscope (Zeiss) and AxioCam HRc camera (Zeiss).

Western blot. One million to two million cells were lysed with radio immunoprecipitation assay (RIPA) buffer (50 mM PH7.4 Tris-HCl, 150 mM NaCl, 1 mM EDTA,1% NP-40, 1% sodium deoxycholate and 0.1% SDS) containing protease and phosphatase inhibitors (Roche). Primary antibodies for Pten (Cell Signaling), Akt (Cell Signaling), phospho-Akt^{S473} and phospho-Akt^{T308} (Cell Signaling), phospho-JNK$^{T183/Y185}$ (Cell Signaling), phospho-Erk1/2 (Cell Signaling), Erk1/2 (Santa Cruz), Ets2 (M.C.O. laboratory) and Collagen 1 (Abcam) were incubated overnight at a dilution of 1:1,000, whereas tubulin (Sigma) was used at 1:5,000 dilution. Washed membranes were blotted with either horseradish-peroxidase-conjugated anti mouse IgG or anti rabbit IgG antibodies and developed with enhanced chemiluminescent substrate (Thermo Scientific).

Microarray analysis. The data were analysed using WEDGE++ expression analysis[52]. Heat map representation (Supplementary Fig. 6) was performed using the TIGR Multiexperiment Viewer program MeV version 4.1.

Quantitative RT–PCR. Quantitative gene expression was performed using 50 ng complementary DNA per reaction. Taqman Roche Universal Probe Library system probe and primers (Roche) following the manufacturer's instructions. Reactions were performed on the I-cycler iQ Real-Time machine (Bio-Rad). A list of quantitative RT–PCR primers can be found in Supplementary Table 3. The reference gene used for all quantitative RT–PCR assays is *Rpl4*.

ChIP and quantitative RT–PCR. ChIP assays were performed as described by Hu *et al.*[53]. Primary fibroblasts were cross-linked with 1% formaldehyde and soluble chromatin was prepared with sonication to an average DNA length of 200–1,000 base pairs. Sheared soluble chromatin was pre-cleared with transfer-RNA-blocked Protein G Agarose, and 10% of the pre-cleared chromatin was set aside as input control. Immunoprecipitation was performed with 5 μg of Ets2 antibody or rabbit IgG overnight at 4 °C. Immune complexes were pulled down with Protein G-Agarose, washed, and eluted with elution buffer (0.1 M NaHCO3, 1% SDS), and cross-links removed by incubating with 200 mM NaCl containing 50 μg ml^{-1} of RNase A (Sigma) at 65 °C overnight. DNA was purified with the Qiagen PCR Purification Kit after proteinase K treatment according to the manufacturer's instructions. Samples were analysed by quantitative RT–PCR as indicated above. The threshold for the promoter being studied was adjusted by that of input values and represented as relative abundance. All quantitative RT–PCR reactions were analysed by melt curve analysis and agarose gels to confirm the specificity of the reaction. A list of ChIP primers can be found in Supplementary Table 3.

Generating the human stroma heat map with genes identified in *Pten* null fibroblasts. Analysis of the *Pten* null mouse microarray data using WEDGE++ software[52] led to the identification of 195 differentially expressed probe sets matching to 150 unique mouse genes. A search for human orthologues using Ensembl and MGI databases yielded a list of 137 genes. These genes were queried against the McGill Cancer Center's Breast Stroma Microarray data (GSE9014 and GSE4823). Of the 137 genes, 129 were represented on the Agilent Custom Array used in the McGill study. A heat map was generated for the human stroma data set (52 normal stroma and 49 tumour stroma samples). To achieve better resolution

on the heat map, and to identify only those genes that had highly variable gene expression across all samples, a variance cutoff of >0.5 was used to generate a subset of 70 genes. The heat map (Fig. 5a) shows the ability of these 70 genes to separate the normal and tumour stroma samples based solely on their gene expression profiles. This partitioning is highly significant ($P = 3.9 \times 10^{-15}$), as determined by Wilcoxon's test on the average expression of *Pten* null-signature in all samples.

Interestingly, comparison of 137 human orthologues of the *Pten* null list with the 163 genes associated with recurrence in tumour stroma from the McGill study showed that there are 12 genes (highlighted in red; Fig. 5a) present on both gene lists. This overlap is again highly significant ($P = 2.5 \times 10^{-8}$; Fisher's exact analysis).

TMA. TMA slides containing paraffin-embedded breast carcinoma tissues were processed at the Pathology Core Facility and Tissue Archives Human Tissue Resource Network at Ohio State University. IHC on these slides was performed with phospho-Ets2^{T72} (1:25, M.C.O. laboratory), Pten (1:100, Cell Signaling) and phospho-Akt^{S473} (1:50, Cell Signaling) following standard procedures. Level of PTEN and phospho-ETS2 and phospho-AKT expression in stromal cells were scored with Allred score method[48].

Statistical analysis. The number of animals and experiments are indicated in the figures. All the statistical tests were two-sided. The Wilcoxon rank test was used for some of the statistical analyses when the outcome variables were skewed and could not be transformed to achieve normality (Figs 1f and 2c, e, i). General linear models (analysis of variance) were used to study differences in continuous outcome variables among groups. *Ad hoc* pairwise comparisons were performed if the overall test was significant (Fig. 4b, d, f and Supplementary Figs 9c and 11b). Fisher's exact test was used to compare counts in Fig. 1e because low counts (below 5) were observed in one of the groups. Fisher's exact test was also used to compare gene overlap in Fig. 5b. Multiplicity adjustment methods (Bonferroni method) were used when multiple pairwise comparisons were performed. A two-sample (unpaired) Student's *t*-test was used for tumour load and the fluorescent microscopy images of $VEGF_{164}$, CD31 and pVEGFR^{Y1173} staining in Fig. 3b, e, f and Supplementary Fig. 9a, e. For human TMA, a Pearson correlation was used to evaluate the association of Allred scores between PTEN/P-ETS2^{T72}, PTEN/P-AKT^{S473} and P-ETS2^{T72}/P-AKT^{S473}.

We show the expression data comparing normal and tumour stroma in Fig. 5a as a heat map because it highlights the 'direction' of the change in expression. Moreover, a permutation test strategy was used to study whether the 70-gene subset of the mouse Pten signature discriminated between human tumour and normal stroma samples[54] (Fig. 5a). A total of 100,000 random permuted samples was used to compute the empirical *P* value of the 70-gene signature. A Wilcoxon rank sum value for each random 70-gene permutation was computed from the average log expression difference (between normal and tumour stroma) of the 70 genes. For computing the average log expression difference of the mouse Pten 70-gene signature, we assigned negative values to the 13 downregulated genes. The empirical *P* value obtained using this method (8×10^{-5}) represents the proportion of random permuted samples that had a Wilcoxon rank sum value larger than the Wilcoxon rank sum value of the Pten 70-gene unpermuted signature. In addition, principal component analysis was used to explore whether the Pten 70-gene signature discriminated normal versus tumour stroma; this principal component analysis, like the heatmap presented in Fig. 5a, showed perfect separation of normal and tumour samples (data not shown), with the first component being sufficient for this separation. A Wilcoxon rank sum test yielded a *P* value of less than 1×10^{-10}.

50. Soriano, P. Generalized lacZ expression with the ROSA26 Cre reporter strain. *Nature Genet.* **21,** 70–71 (1999).
51. Mook, O. R., Van Overbeek, C., Ackema, E. G., Van Maldegem, F. & Frederiks, W. M. *In situ* localization of gelatinolytic activity in the extracellular matrix of metastases of colon cancer in rat liver using quenched fluorogenic DQ-gelatin. *J. Histochem. Cytochem.* **51,** 821–829 (2003).
52. Auer, H. *et al.* Gene-resolution analysis of DNA copy number variation using oligonucleotide expression microarrays. *BMC Genomics* **8,** 111 (2007).
53. Hu, R. *et al.* Eos, MITF, and PU.1 recruit corepressors to osteoclast-specific genes in committed myeloid progenitors. *Mol. Cell. Biol.* **27,** 4018–4027 (2007).
54. Westall, P. H. & Young, S. S. *Resampling-Based Multiple Testing: Examples and Methods for p-Value Adjustment* (John Wiley, 1993).